†Deceased 30 May 2021

Key Points:
- A remarkable observational evidence of onset of plasma depletions is captured over geomagnetic transition region in a span of 25 min
- It is argued that both mid-latitude sporadic-E layer and Perkins instabilities are simultaneously needed to explain the growth time
- It is also proposed that reduced flux tube integrated Pedersen conductivity over south of onset location favored the growth of the bubble

Supporting Information:
Supporting Information may be found in the online version of this article.

Correspondence to:
S. Sarkhel,
sarkhel@ph.iitr.ac.in

Evidence for the In-Situ Generation of Plasma Depletion Structures Over the Transition Region of Geomagnetic Low-Mid Latitude

M. Sivakandan[1,2] , S. Mondal[3] , S. Sarkhel[3] , D. Chakrabarty[4] , M. V. Sunil Krishna[3] , A. K. Upadhayaya[5] , A. Shinbori[1] , T. Sori[1] , S. Kannaujiya[6] , and P. K. Champati Ray[6],†

[1]Institute for Space-Earth Environment Research (ISEE), Nagoya University, Nagoya, Japan, [2]Now at Leibniz Institute of Atmospheric Physics (IAP) at the University of Rostock, Kühlungsborn, Germany, [3]Department of Physics, Indian Institute of Technology Roorkee, Roorkee, India, [4]Space and Atmospheric Sciences Division, Physical Research Laboratory, Ahmedabad, India, [5]Environmental Sciences and Biomedical Metrology Division, CSIR National Physical Laboratory, New Delhi, India, [6]Indian Institute of Remote Sensing, ISRO, Dehradun, India

Abstract On a geomagnetic quiet night of October 29, 2018, we captured an observational evidence of the onset of dark band structures within the field-of-view of an all-sky airglow imager operating at 630.0 nm over a geomagnetic low-mid latitude transition region, Hanle, Leh Ladakh. Simultaneous ionosonde observations over New Delhi shows the occurrence of spread-F in the ionograms. Additionally, virtual and peak height indicate vertical upliftment in the F layer altitude and reduction in the ionospheric peak frequency were also observed when the dark band pass through the ionosonde location. All these results confirmed that the observed depletions are indeed associated with ionospheric F region plasma irregularities. The rate of total electron content index (ROTI) indicates the absence of plasma bubble activities over the equatorial/low latitude region which confirms that the observed event is a mid-latitude plasma depletion. Our calculations reveal that the growth time of the plasma depletion is ~2 h if one considers only the Perkins instability mechanism. This is not consistent with the present observations as the plasma depletion developed within ~25 min. By invoking possible Es layer instabilities and associated E-F region coupling, we show that the growth rate increases roughly by an order of magnitude. This strongly suggests that the Cosgrove and Tsunoda mechanism may be simultaneously operational in this case. Furthermore, it is also suggested that reduced F region flux-tube integrated conductivity in the southern part of onset region created conducive background conditions for the growth of the plasma depletion on this night.

Plain Language Summary It is well known that the plasma irregularities/depletions in the ionosphere degrade the satellite-based communication navigation signals, significantly. Thus, understanding the plausible onset condition and characteristics of these depletions are vital for the better space weather forecasting. Occurrence of plasma depletion in the equatorial and high latitude regions are associated with Generalized Rayleigh Taylor instability mechanism and their characteristics are mostly well reported. On the other hand, though the characteristics of the mid-latitude field aligned irregularities are reported by a few investigators, there is no direct observational evidence for the onset of the mid-latitude plasma depletion till now. Thus, the present investigation provides first optical observational evidence of in-situ generation of plasma depletion and provides some insight on the possible background conditions which supported the onset over the geomagnetic low-mid latitude transition region.

1. Introduction

F-region plasma depletion structures and the associated dark bands in the O (^{1}D) 630.0 nm airglow images is frequently observed in the post-sunset hours during the equinoctial months and in the post-midnight hours during the solstice (i.e., June and July) in the high and low solar activity years over the equatorial and low-latitude sectors (particularly Asian sector), respectively. These plasma depletion structures are commonly referred as equatorial plasma bubbles (EPB) (e.g., Otsuka, 2018; Patra et al., 2009; Paulino et al., 2011; Taori & Sindhya, 2014; Yao and Makela, 2007) or historically as Equatorial Spread F (ESF) because of the associated spread in range and/or frequency in the return echo captured by an ionogram. As

the F region plasma, to a good approximation, is considered "incompressible" (e.g., Kelley, 2009). The term "plasma depletion structure" does not, in any way, suggests the reduction in the total plasma density in the F region. Although the signatures of plasma depletions in the vertical total electron content (VTEC) or in thermospheric airglow images are observed, it is obvious that these are signatures of localized changes in the plasma density and the F region plasma density, as a whole, does not change. The plasma merely gets redistributed and this was suggested based on two-dimensional non-linear numerical simulation results by Sekar et al. (2001) when they predicted presence of plasma enhancement structure alongside the depletion structure. This was later experimentally verified by coordinated VHF radar and narrow spectral band (0.3 nm) and narrow field-of-view (FOV) photometry (Sekar & Chakrabarty, 2011; Sekar et al., 2004, 2008). Therefore, the term "plasma depletion structure" used in the present work is not intended to violate the general "incompressibility" assumption of the F region plasma and is used only for ease of comprehension of the research community.

About half a century ago, it was believed that the irregularities in the ionospheric electron densities were highly confined to the equatorial and high-latitude regions where the geomagnetic field lines are aligned parallel and perpendicular to the surface of the Earth respectively. It is now known that the causative mechanism of EPB is the Rayleigh Taylor (RT) instability (Chiu & Straus, 1979; Huang & Kelley, 1996; McClure et al., 1977; Tsunoda et al., 1982; Woodman & La Hoz, 1976). On the other hand, the mid-latitude ionosphere was considered as quiescent in nature a few decades back. However, from the early 70's, advancement in the ionosonde and incoherent radar (particularly, the MU radar and Arecibo radar) observations revealed that ionospheric irregularities can occur even in the mid latitudes (Fukao et al., 1991; Mathews et al., 2001; Miller et al., 1997; Swartz et al., 2000), particularly during the solstice months and the RT mechanism fails to explain the growth of these instabilities. It was proposed that Perkins instability could be a plausible causative mechanism of mid-latitude spread-F. According to the Perkins theory (Perkins, 1973), change in eastward electric field and/or southward wind in the mid-latitude ionosphere can disturb the plasma equilibrium against the Earth's gravity giving rise to plasma instability structures. One drawback of the Perkins instability is that the growth rate is very small (Shiokawa, Otsuka, et al., 2003). Studies also suggest that E region coupling with F region could enhance the growth of the Perkins instability (e.g., Cosgrove, 2007, 2013; Cosgrove & Tsunoda, 2001, 2003, 2004; Cosgrove et al., 2004; Earle et al., 2010; Haldoupis et al., 2003; Hysell et al., 2018; Otsuka et al., 2008; Tsunoda & Cosgrove, 2001). Furthermore, model simulation showed that polarization electric fields associated with the sporadic Es patches with scale size more than 10 km can effectively map into the F region and it can cause the irregularities in the F region irrespective of Perkins instability condition (Shalimov & Yamamoto, 2010).

Two distinct kinds of electric field fluctuations are observed in the mid-latitude ionosphere such as, electric field fluctuations associated with (a) Nighttime medium scale traveling ionospheric disturbances (MSTIDs) that mostly appears at the conjugate points of the ionosphere (Saito et al., 1995) simultaneously, (b) Mid-latitude F-region field aligned irregularities (FAIs) observed by the incoherent scatter radar (Fukao et al., 1991; Otsuka et al., 2009). MSTIDs propagate toward southwest with northwest to southeast phase front alignment (Narayanan et al., 2014; Rathi et al., 2021 and reference therein). On the other hand, FAI drifts westward (Fukao et al., 1991; Hysell et al., 2016, 2018) and plasma moves upward inside FAI structures. Although the MSTIDs and mid-latitude FAIs are two different phenomena believed to be triggered by the Perkins instability mechanism, various aspects like the equatorward-westward propagation of the MSTIDs, growth rate etc. could not be explained satisfactorily. Recently Hysell et al. (2016) suggested a combination of interchange-type plasma instability and Kelvin Helmholtz type plasma instability can explain the mid-latitude spread-F structures observed over Arecibo. More importantly, the e-folding time for these processes appear to be much shorter than that predicted for Perkins instability.

Using various ground based and satellite measurements such as Ionosonde, radar, Global Positioning System total electron content (GPS-TEC) and airglow imager etc., characteristics of electrified MSTIDs (Behnke, 1979; Bowman, 1990; Bowman & Monro, 1988; Ding et al., 2011; Otsuka et al., 2009; Shiokawa, Ihara, et al., 2003; Tsugawa et al., 2007) and FAIs (Haldoupis et al., 2003; Hysell et al., 2016; Larsen et al., 2007; Mathews et al., 2001; Saito et al., 2008; Sun et al., 2015) are reported in the literature extensively. However, onset of MSTID or FAI in the FOV of an airglow imager are not reported to the best of our knowledge. These events have the potential to throw light on the background conditions that are instrumental in

triggering plasma instabilities. This assumes much more importance in the context of the transition region of the low and mid latitudes as there can be competing influences of the low and mid-latitude processes in determining the favorable generation condition and evolution of plasma irregularity structures over this region. In the present study, such an observational evidence of the onset of mid-latitude FAI over the transition region of low and mid latitudes is presented and the possible causative mechanisms are investigated.

2. Data Set

Using the simultaneous optical and radio measurements such as all-sky airglow imager, ionosonde, and Global Navigation Satellite System (GNSS), onset of a plasma depletion over Hanle a low-mid latitude transition region is studied. A brief description of these instruments are as follows:

2.1. Airglow Imaging

An all-sky airglow imager over Hanle, Leh Ladakh (32.7°N, 78.9°E; Mlat. ~24.1°N; Apex ~1,575 km; Height: ~4,200 m above the mean sea level), a transition region of geomagnetic low and mid latitudes measures O (^{1}D) 630.0 nm (peak emission altitude ~250 km) airglow emissions to investigate and characterize the F-region ionospheric plasma instabilities. The detailed descriptions of the all-sky imager with an effective FOV of ~140°, image processing techniques and first results are available in literature (Mondal et al., 2019). In the present study, O (^{1}D) 630.0 nm airglow emission data are utilized.

2.2. Ionosonde Observations

Ionosonde observation from New Delhi (28.70°N, 77.10°E; Mlat. ~20.2°N; Apex ~1,146 km, northern/poleward edge of the crest region of Equatorial Ionization Anomaly [EIA]) is used to investigate the spread-F occurrence over the low-mid latitude transition region. Since the location of the ionosonde observation is partially covered by the all-sky imager FOV, this data can be used to confirm whether the airglow depletions are associated with plasma irregularities or not. Details of the New Delhi ionosonde is available in Upadhayaya and Mahajan (2013).

3. Results

3.1. Observation of the Appearance of Dark Bands in the FOV of the All-Sky Imager

On the night of October 29, 2018 (a geomagnetic quiet night), in-situ generation of two dark band structures were observed in the O (^{1}D) 630.0 nm airglow images over Hanle, Leh Ladakh, a transition region of low and mid-latitude over the Indian Himalayan region. It should be noted here that there is no defined magnetic low mid-latitude transition region in the literature. Here we assume that the region between 20 and 30° geomagnetic latitude (corresponding Apex altitude range is 1,127–2,457 km) as low mid-latitude transition region. Few sample 630.0 nm airglow images on October 28, 2018 (top panel) and October 29, 2018 (middle and bottom panels) are depicted in the Figure 1. On October 28, 2018, the imager was operated only up to 14:58 UT and during this period, there is no dark band observed. In Figure 1, all the images are overlaid on the map of the northern part of the Indian subcontinent. In these images, the geomagnetic declination angle is marked by a red dotted line, the airglow imager location is denoted by red star and the New Delhi ionosonde location is indicated by red triangle. We encourage the readers to go through the complete sequence of images (October 29, 2018) which is reproduced in the form of a movie and available in the Movie S1. On this night, airglow observations over Hanle were carried out from ~14:00 to 16:00 UT (Universal Time). Afterward, the operation was ceased due to moonlight. For the first 20 min (i.e., from the starting time to 14:20 UT), there is no depletion observed in the images. After that a dark region is developed in the southeastern part of the image at 14:24 UT, followed by a mild dark band structure appeared in the next image that is, 14:30 UT. In the consecutive images, the dark band structure became more prominent at around 14:49 UT with ~10% perturbation in the relative intensity and continued till end of the observation (i.e., 15:58 UT see Figures 2a and 2b). It can be noted that the dark band structure, developed within around 25 min, is aligned in the northwest to southeast direction with tilt angle of ~35° west from the geomagnetic north. In the mid latitudes (northern hemisphere), northwest to southeast phase front with southwest moving structures are
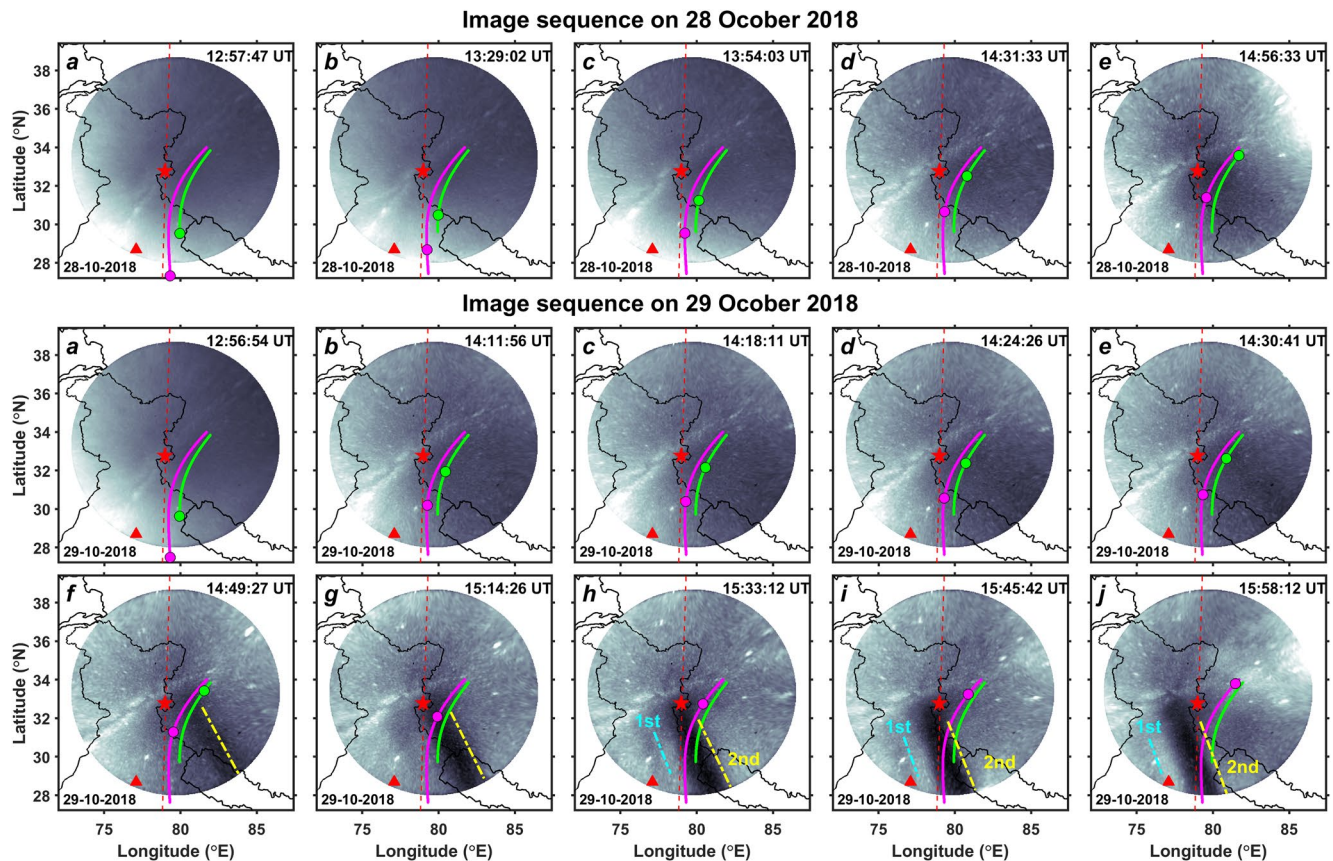
Figure 1. Sequence of 630.0 nm airglow images on 28 (top panel), 29 (middle and bottom panels) October 2018. In the images, the locations of the imager (Hanle) and the ionosonde (New Delhi) are represented by the red colored star and triangle respectively. The red dotted line represents the geomagnetic field line. The Global Navigation Satellite System satellite passes PRNs 16 and 26 are shown in magenta and green color respectively and the magenta and green dots represent the PRN positions at that particular time.

frequently observed during the summer and/or winter nighttime which are known as electrified MSTIDs (EMSTIDs) and move toward southwest. However, in the present case, the dark band structure was not moving toward southwest. Instead, it is drifted toward west. Therefore, it is reasonable to believe that the noted event is not EMSTIDs. In the beginning, only one dark band is noticed till 14:55 UT. Later on, another a weak dark band structure is also generated ahead of the first one at 15:08 UT onward (hereafter the weak dark band and strong dark band is named as depletion 1 and 2 respectively). In Figure 1, the depletions 1 and 2 are highlighted by the blue and yellow dotted lines respectively. However, no such dark bands were observed on the previous night that is, October 28, 2018. The drift velocities of the strong and weak dark band structures calculated from the consecutive images are 79 ± 9 m/s and 79.5 ± 2 m/s respectively.

3.2. GNSS VTEC Variation Over Mandi

Furthermore, in order to understand the VTEC variation around the dark band region if any, single satellite pass over the dark band region is investigated. The VTEC measurements were carried out by a GNSS receiver installed at Mandi (30.45°N, 79.27°E) which is located in the southern side of Hanle covered by the FOV of the imager. We found that there are two satellite PRNs namely PRN 16 and PRN 26 passed across the depletion 2. Therefore, those two PRNs passage over the FOV of the image on that night is also plotted in Figure 1. In Figure 1, PRNs 16 and 26 are shown in magenta and green color respectively and the magenta and green dots represent the PRN position at that particular time.

In order to understand the simultaneous VTEC and airglow intensity perturbations, we compared the VTEC perturbation with airglow intensity perturbation at 15:33:12 UT. Airglow image at 15:33:12 UT and airglow
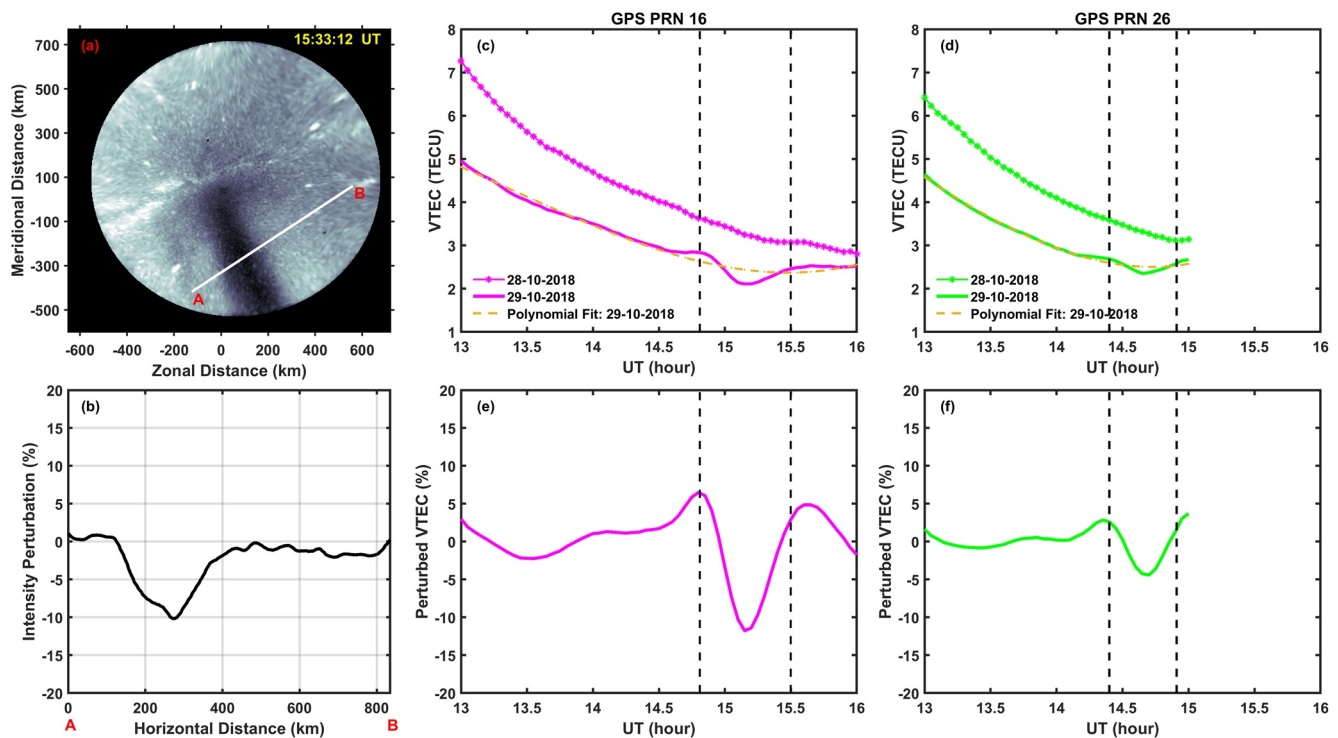
Figure 2. (a) Depletion in the airglow intensity at 15:33:12 UT and PRNs 16 and 26 passage close and/or across the depletion during this time is also shown in magenta and green respectively. (b) The airglow intensity depletion along the PRN 16 passage. (c) and (d) Vertical total electron content (VTEC) variation of single satellite pass across the field-of-view images on the control (October 28, 2018) and event (October 29, 2018) day. (e) and (f) Perturbed VTEC of PRN 16 and 26 on the event day is plotted respectively.

intensity perturbations are shown in Figures 2a and 2b respectively. PRNs 16 and 26 VTEC variation (elevation angle 30° and above are considered for the total electron content [TEC] calculation) on October 29, 2018 are plotted in Figures 2c and 2d and their perturbations are plotted in Figures 2e and 2f. It is to be noted that VTEC for both the PRNs are bias corrected. It is obvious that a small reduction in the VTEC is observed around 14:45 and 15:15 UT for PRNs 26 and 16 respectively. It should be noted that this is the time when the PRNs passage coincide with the dark band structure. In order to estimate the VTEC perturbation, first a fourth order polynomial fit is carried out then the fitted VTEC is subtracted from the actual VTEC and obtained result is shown in Figures 2c and 2d. Figure 2e clearly shows that around 10% perturbation in the TEC. This evidently shows the reduction in the TEC during the dark band structure occurrence. This gives a hint that the dark band structure may be partially supported by the reduction of the electron density in the F region.

3.3. ROTI Maps

We have confirmed the absence of the FAIs on this night based on 30 MHz HF radar range-time-intensity (RTI) map over Gadanki (a low latitude station). In order to provide an addition support on the absence of ESF occurrence, the rate of TEC index (ROTI) maps over the equatorial sector are also used. Figure 3 shows the ROTI maps from 15:00 UT to 17:45 UT, that is, duration at which the onset of plasma depletion observed over Hanle. In general, ROTI magnitude is more than 0.25 TECU/min can be considered to be indicative of EPB occurrence (Ji et al., 2015). During the above-mentioned interval, the ROTI value is always less than 0.25. It indicates that there is no scintillations over the geomagnetic low latitude/equator. These results suggest that the observed dark bands are not associated with the EPBs.
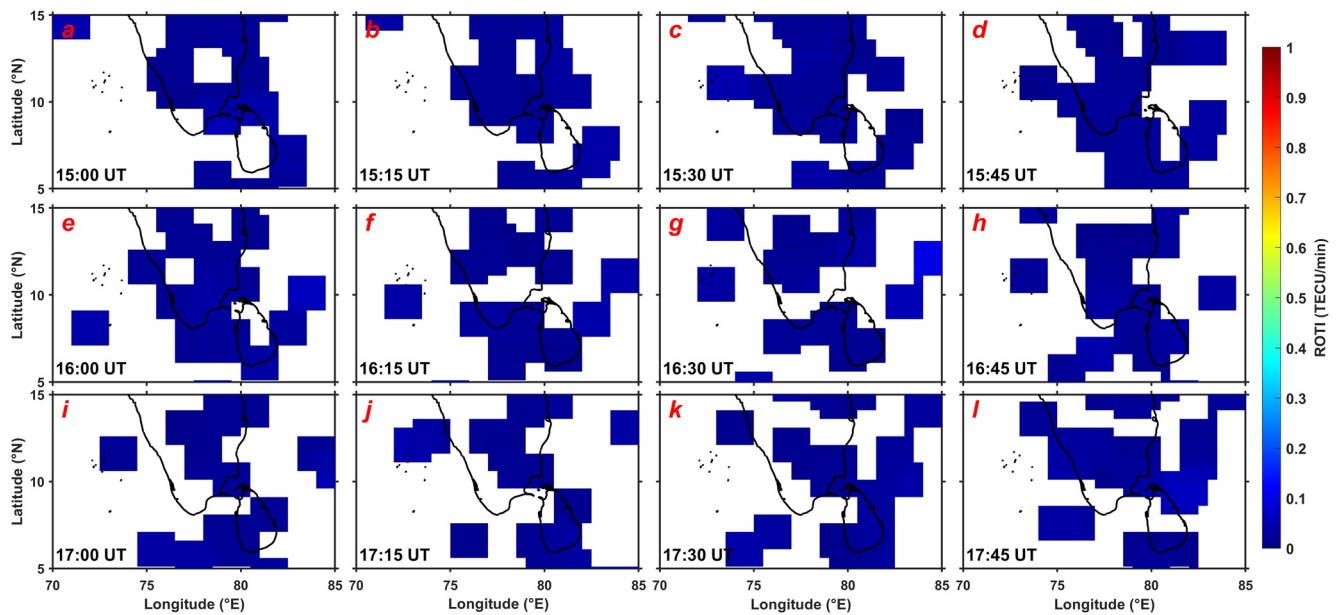
Figure 3. Rate of total electron content index (ROTI) maps over the geomagnetic equatorial and low-latitude region from 15:00 to 17:45 UT on October 29, 2018.

3.4. Ionosonde Observation From New Delhi

In order to investigate the occurrence of spread-F in the low and mid-latitude transition region ionosonde observation from New Delhi is used. It is located poleward side of the EIA crest and the ionosonde beam at New Delhi overlaps with the FOV of the Hanle all-sky imager at the southern fringe of the airglow image captured from Hanle. A Few consecutive ionograms for October 28, 2018 and October 29, 2018 are shown in Figure 4. The ionogram on the night of October 28, 2018 did not show any spread-F signatures even up to 17:00 UT. However, in the next night (October 29, 2019), the ionosonde observations show mild range spread-F signatures in the ionograms at 16:05 UT onwards. It is interesting to note that the first dark band passed over the ionosonde location at 15:51 UT on this night. Due to the 15 min cadence of ionosonde observations, the spread-F is noted at 16:05 UT but no spread-F is observed at 16:20 UT. Afterward, an intense spread-F is observed in the ionograms from 16:35 UT till 19:05 UT (this is the time when the depletion 2 passed over the ionosonde location). This supports that the dark patch observed in the airglow observation is indeed a spread-F structure. However, it must be noted at this point that the occurrence of Es signatures and the upliftment of F layer can also be observed on both the nights after 14:30 UT over New Delhi. We will discuss the importance of low latitude TEC in the context of these observations in the ensuing section.

4. Discussion

Onset of two dark bands were captured in the O (^{1}D) 630.0 nm airglow images over Hanle, a geomagnetic low-mid latitude transition region, on October 29, 2018. Initially a dark region is observed in the southeastern part (below the 24.1°Mlat) of the airglow image and within 20 min, a dark band structure is developed in the images. Subsequently, another weak dark band is also generated in the western side of the first dark band. Both the dark band structures are elongated in the northwest to southeast direction and drift toward west. Interestingly, no such events are noted on the previous night that is, October 28, 2018 in the 630.0 nm airglow images over Hanle (due to the moon rise the observation available only up to 13:00 UT). The dark band/depletion structure is noted only southern part of Hanle, that is, below 24.1°N Mlat. A statistical study over the South-Asian sector showed that the maximum magnetic latitudinal extension of EPB is usually lower than 15.0° (apex altitude ~725 km), but it can reach up to 23.0° (apex height ~1,330 km) when F10.7 > 140 (Sun et al., 2016). Therefore, in order to assess whether the dark bands are originated from the equatorial region or generated over the low-mid latitude transition region, ROTI maps over the geomagnetic equatorial and low latitude region are verified. ROTI values are always less than 0.2 TECU/min, this
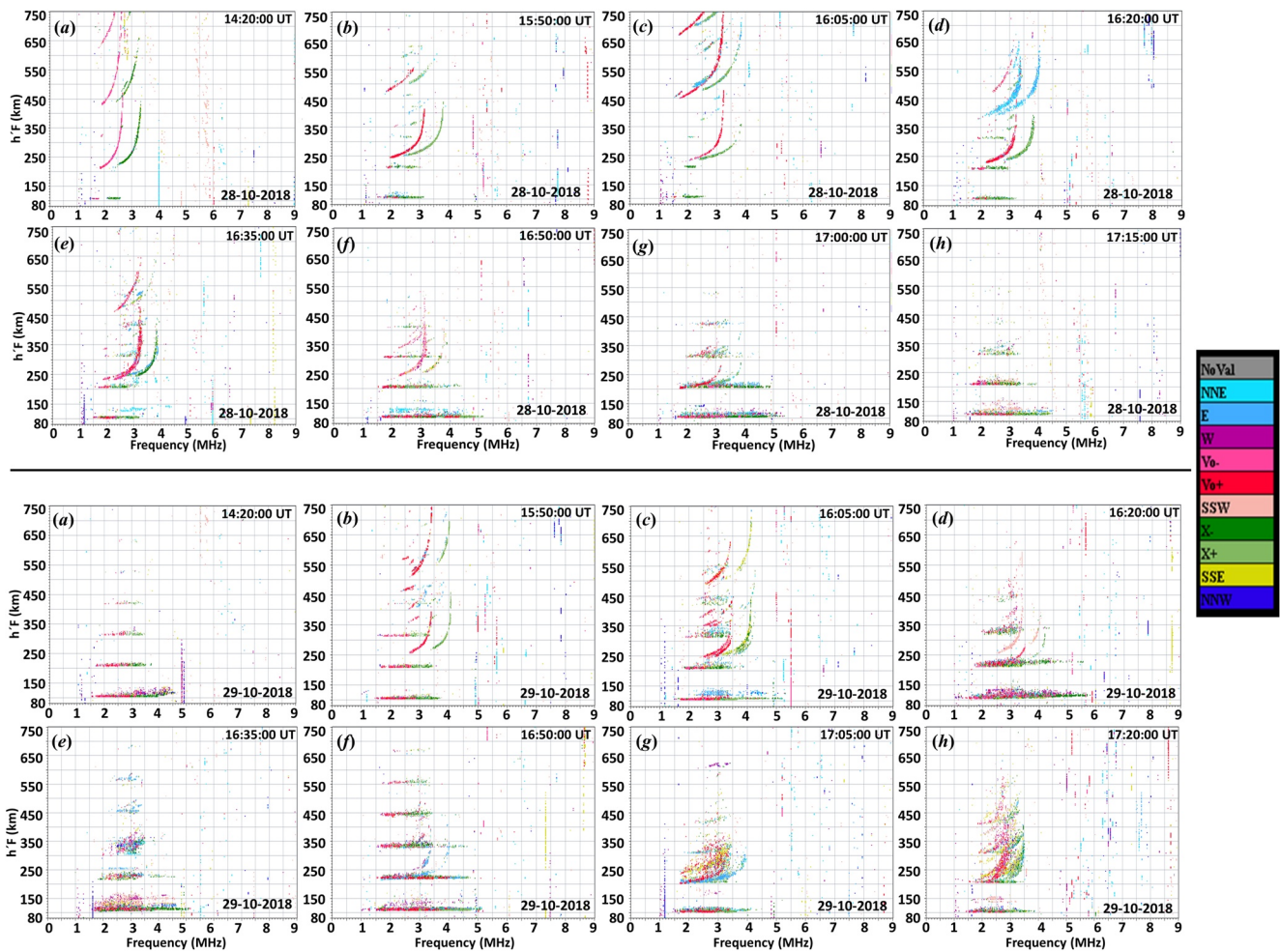
Figure 4. Sequence of ionograms over New Delhi from 14:20 to 17:20 UT on October 28 and 29, 2018.

indicates that there are no small-scale irregularities. It is to be noted here that in solar maximum years, the absence of GPS scintillations would automatically indicate the absence of EPBs, but during solar minimum years this cannot be taken for granted (due to the possibility of EPB without GPS scintillation). During solar minimum years, EPBs often do not cause GPS scintillations because the background TEC is too low and hence there are not enough density irregularities within the EPBs. Low values of ROTI or S4 index indicate the absence of ionospheric plasma density irregularities. Thus, additionally we also looked in to the RTI maps of 30 MHz radar over Gadanki a low latitude station. The RTI map also did not show any irregularities structures. Therefore, combination of low ROTI and the absence of FAI over Gadanki certainly indicate that there was no EPBs on the night of October 29, 2018 over the area. This supports that the observed structure is confined within the geomagnetic low-mid latitude transition region only and the westward drift suggest that this may be associated with the mid-latitude phenomena. As explained in the Introduction section that there are two kinds of phenomena which can cause dark band in the 630.0 nm airglow images that is, (a) EMSTIDs and (b) mid-latitude spread-F/plasma depletion. Since the proposed generation mechanisms for both of these events are the same (i.e., Perkins instability), thus sometimes it is hard to distinguish them. However, in a statistical study by combing the airglow observation and radar measurements, Shiokawa, Ihara, et al. (2003) showed that 15% of time MSTIDs observed in the airglow emission without FAIs in Middle and Upper atmosphere radar. Based on this result, they argued that these two phenomena are different from each other. Keeping this investigation in mind, we tried to distinguish the observed dark band whether it is onset of MSTID or mid-latitude plasma depletion. In the present investigation, the dark band structures are tilted by ~35° toward west from the geomagnetic north which is similar to the EMSITDs, however the
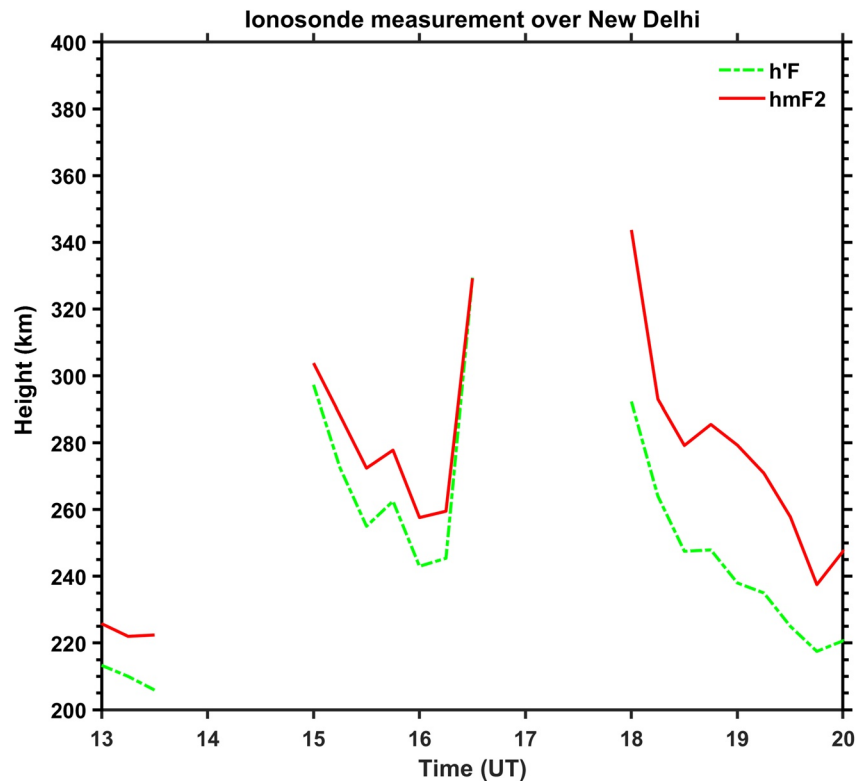
Figure 5. Ionosonde observation of virtual (h'F) and peak height (hmF2) over New Delhi.

structure drifted toward west instead of southwest (which is mid-latitude EMSTID propagation direction in the northern hemisphere). Furthermore, most often the MSTIDs used to have minimum three to four consecutive bright and dark bands within the FOV but in the present case we just noticed only two dark bands. These points suggest that the observed dark bands are associated with plasma depletion.

In general, a sharp reduction of plasma/electron density observed in the ionosphere (particularly in the equatorial and low latitude region) is called as "plasma depletion." In this context, an important point to be mentioned here that O (^{1}D) 630.0 nm intensity reduction/dark band appearance need not to be reduction in the plasma density. As it is well known that the O (^{1}D) 630.0 nm emission arises from the dissociative recombination mechanism that is,

$$O^+ + O_2 \rightarrow O_2^+ + O \tag{1}$$

$$O_2^+ + e^- \rightarrow O^* + O \tag{2}$$

Here O* (O (^{1}D) or O (^{1}S)) is excited state of atomic oxygen. From Equations 1 and 2, it is clear that the O (^{1}D) 630.0 nm emission rate (intensity) is not only depends on the electron density (e$^-$), it also depends on the molecular oxygen (O$_2$) density. Owing to this dependence on (O$_2$), the peak of the emission typically occurs about a scale height below the F peak, therefore the dimming (brightening) of the emission can be due to either decrease (increase) of the electron density or the raising (lowering) of the F layer as a whole (Makela & Kelley, 2003; Makela et al., 2001). In order to ascertain the plausible causative mechanism of the observed dark band in the airglow images, ionosonde measured virtual base height (h'F) and ionospheric peak height (hmF2) variations are investigated and that is shown in Figure 5. As mentioned in the data set section, ionosonde is located southwest of Hanle and it is partially covered by the FOV (location of New Delhi is shown in the Figure 1) of the airglow imager. Ionosonde h'F and hmF2 show a small raise in altitude at 15:45 UT and a sharp rise in the altitude at 16:30 UT onwards. Furthermore, GPS VTEC also shows a small reduction in the VTEC and the percentage of TEC and airglow intensity reduction are comparable when the PRNs passed over the dark band structure (shown in Figure 2). These results confirm that the observed dark band is combination of upliftment of F layer and reduction in electron density. We strongly

feel that it is unlikely that the uplifting (and not depletion, let us say) of F layer happens in a narrow, localized region so that it changes the recombination condition and changes VTEC. In that case, changes in VTEC (it should increase due to reduced recombination/quenching processes) are expected to spread over a large spatial region and should get reflected in all the PRNs. This has not happened in this case and the signatures are clearly visible only in PRN 16 and PRN 26 that cut across the dark intensity band observed in the airglow image. Therefore, as per Figure 2, the simultaneous presence of dark band and the dip in VTEC strongly suggest that this is a plasma depletion region. Therefore, we believe that using the term "plasma depletion structures" is more reasonable than dark bands (hereafter the term "dark band" is replaced with "plasma depletion"). In order to verify whether the observed event is airglow depletion alone or associated with the spread-F, ionograms over New Delhi are investigated. The ionograms show a range spread-F from 16:05 UT to 19:05 UT. It is interesting to note that no spread-F is observed at 16:20 UT. As mentioned in the result section, there are two depletion structures in the images: the first one (weak depletion) reached to the ionosonde location at ∼15:50 UT and the second depletion (deep depletion) reached after 16:30 UT. Thus, it confirms that the spread-F noticed in the ionograms at 16:05 UT is the representation of the weak depletion and the strong range spread from 16:35 UT onwards is representation of the strong depletion. Moreover, the absence of spread-F at 16:20 UT over New Delhi is due to the spatial separation between the two depletions.

Earlier investigation showed that the mid-latitude spread-F can be caused by the presence of wave undulation in the ionosphere alone or combination of E and F region coupling processes (Cosgrove, 2013 and reference therein; Earle et al., 2010). Recently, Sivakandan et al. (2020); Yadav, Rathi, Gaur, et al. (2021), and Yadav, Rathi, Sarkhel, et al. (2021) observed a mid-latitude spread-F/field aligned plasma structures over the low-mid-latitude transition region, Hanle and argued the possible supporting mechanism. However, to the best of our knowledge, there is no observational evidence that shows the onset and evolution of plasma depletion in the FOV of an airglow imager over the geomagnetic low-mid latitude transition region. In the subsequent section, we explore the possible factors that might have influenced the in-situ generation of plasma bubble on this night.

4.1. Role of Coupled Perkins and Es Instability in the Onset of Depletion

Perkins instability is believed to be the causative mechanism for the generation of FAI and/or EMSTIDs in the mid-latitude region (in the original Perkins theory E region contribution to the F region conductivities are neglected). The maximum growth rate (γ_{max}) of the Perkins instability (Perkins, 1973) is

$$\gamma_{max} \approx 3 \times 10^{-4} \times \frac{\sin^2 D \times \sin^2\left(\frac{\theta}{2}\right)}{\langle \vartheta_{in} \rangle \cos \theta} \tag{3}$$

It significantly depends on the dip angle D, the angle between geographic east and the electric field vector (θ) and ion-neutral collision frequency $\left(\vartheta_{in}\right)$. The maximum growth rate occurs for $\alpha = \theta/2$, where α is the angle between geographic east and wave vector that is ∼211° for the current event. In the present case, D is estimated using the IGRF model that is 47.05° (at 30°N; 83°E where the onset of dark band is observed). The ion-neutral frequency is calculated using the MSIS model neutral densities that is 0.645/s at 250 km. The estimated maximum growth rate of the observed event is ∼$1.38 \times 10^{-4} s^{-1}$ (i.e., 2 h). Thus, according to the classical Perkins theory, it will take a minimum of ∼2 h for the depletion to develop in the present event. However, airglow images shows that a dark region was developed at 14:24 UT and a depletion structure is clearly visible at 14:49 UT, that mean the depletion is fully formed within 25 min. This indicates for the present event the Perkins instability alone cannot explain the faster growth of the observed depletion structure. Numerical simulations by Cosgrove et al. (2004) showed that the growth rate of mid-latitude F region instability gets enhanced when the F-region Perkins instability is also coupled with the sporadic E (Es) layer instabilities. It should be noted here that the E layer conductivity can play an important role in determining the bubble growth rate at the F layer. This is despite the fact that the field line integrated F region conductivity is larger than that of the Es layer. Having larger flux-tube integrated conductivity, the F layer is in a position to exert larger influence on short-circuiting the polarization field associated with the Es layer instability. In spite of that, the integrated Hall conductance (which is the driving source for the polarization electric field in the Es layer) of the dense Es layer can often exceed the integrated Pedersen conductance of the F layer and this makes the Es instability effective in influencing the instabilities at the

F layer heights (Cosgrove & Tsunoda, 2003). This proposition gets further credence from the work of Shalimov and Yamamoto (2010) who showed that Es associated polarization electric fields with scale size more than 10 km can effectively trigger the irregularities in the mid-latitude F region.

Using the Cosgrove et al. (2004) circuit models for E-F coupling, we made an attempt to estimate typical Es instability growth rate contribution for the present case. According to this model, (a) the electric field mapping is wavelength dependent that is, for shorter wavelengths, Es and F layer instabilities are decoupled and for longer wavelengths, these are tightly coupled. (b) The maximum coupled growth rate occurs when the Es and F layer plasma move with same velocity under the influence of winds and background electric fields. The details of the E-F coupling model is available in Cosgrove et al. (2004). The tightly coupled growth rate equation is given below:

$$\gamma_{\mathrm{EFCL}} = \frac{\gamma_{\mathrm{E_s}} R_{\mathrm{F}} + \gamma_{\mathrm{max}} R_{\mathrm{E_S}}}{R_{\mathrm{E_S}} + R_{\mathrm{F}}} \tag{4}$$

In order to find the Es instability, Equation 4 can be rearranged as follows

$$\gamma_{\mathrm{E_s}} = \frac{\left(R_{\mathrm{E_s}} + R_{\mathrm{F}}\right)\gamma_{\mathrm{EFCL}} - \gamma_{\mathrm{max}} R_{\mathrm{E_s}}}{R_{\mathrm{F}}} \tag{5}$$

Here, γ_{EFCL} is the coupled system growth rate (for the present case, it is ~25 min or $6.67 \times 10^{-4}\,\mathrm{s}^{-1}$) whereas, $\gamma_{\mathrm{E_s}}$ and γ_{max} $\left(1.38 \times 10^{-4}\,\mathrm{s}^{-1}\right)$ are Es and Perkins instability growth rates respectively. $R_{\mathrm{E_s}} = 1/\Sigma_{\mathrm{PE}}$ and $R_{\mathrm{F}} = 1/\Sigma_{\mathrm{PF}}$ are Es and F layer internal resistances respectively. In order to calculate the Es layer instability growth rate on this night, we have taken the field line integrated Es layer and F region Pedersen conductivity values from the Cosgrove et al. (2004) work, that is $\Sigma_{\mathrm{PE}} = 0.02$ mhos and $\Sigma_{\mathrm{PF}} = 0.2$ mhos respectively. Based on this calculation, the estimated Es layer instability growth rate turns out to be $6.0 \times 10^{-3}\,\mathrm{s}^{-1}$ or growth time of 2.8 min. This value is comparable with the earlier theoretical estimation by Cosgrove and Tsunoda (2002), in their estimation they showed that 4.2 min as typical growth time of Es instability. Model simulations showed that the growth rate of the F region instability is increased in the presence of Es layer instability (Yokoyama et al., 2009 reference therein). Therefore, Perkins instability provides a much larger growth time and Es layer instabilities render a much smaller growth time if one compares both the growth times with the growth time (25 min) of the bubble suggested by the present observation. Hence, the present observation seems to suggest that both the Perkins instability in the F region and possible Es layer instabilities through E-F region coupling might have simultaneously contributed to the development of the plasma depletion structures within around 25 min on this night. In addition, it is also interesting to note that the observed depletion structure has width of ~200 km on this night (Figure 2a). This larger width of the depletion structure is consistent with Cosgrove et al. (2004) who suggested that larger spatial scale sizes are more effective as far as the E-F region coupling is concerned. All these points indicate that with the presence of Es layer instability and large wavelength seed perturbation along with the Perkins's instability process could enhance the growth rate of the plasma depletion structure observed in the present case. Consistent with this interpretation, strong Es layer is observed in the ionosonde observation over New Delhi (28.7°N) which is located in the southern edge of the imager's FOV. The E region of New Delhi (~100 km) field line maps to the bottom of the F layer (~220 km) at 27.7°N. The present observation suggests that the onset of the plasma depletion occurs somewhere south of New Delhi's latitude as the southern edge of the dark band extend beyond the FOV. From Figure 5, we can observe that the base of the F layer (h'F) has gone upward during 13.5 — 15 UT. Although, the exact altitude of the h'F at time of onset cannot be estimated from ionosonde due to occurrence of blanketing Es layer. However, the dark region is noted around that time in 630.0 nm airglow images which is due to the vertical upliftment of F layer. This provides the conducive background condition for the generation of plasma bubble due to the complex interplay of the Perkins instability in association with the Es layer instability through E-F coupling. This seed perturbation of Es layer polarization electric field due to occurrence of strong Es at New Delhi's latitude played the critical role for the generation of the bubble at the base of F layer (220 km) through field line mapping in the south of New Delhi's latitude. Thus, the present study evidently shows that combination of E and F region instability processes that has the potential to accelerate the growth of plasma depletion over the transition region geomagnetic of the low-mid latitudes.
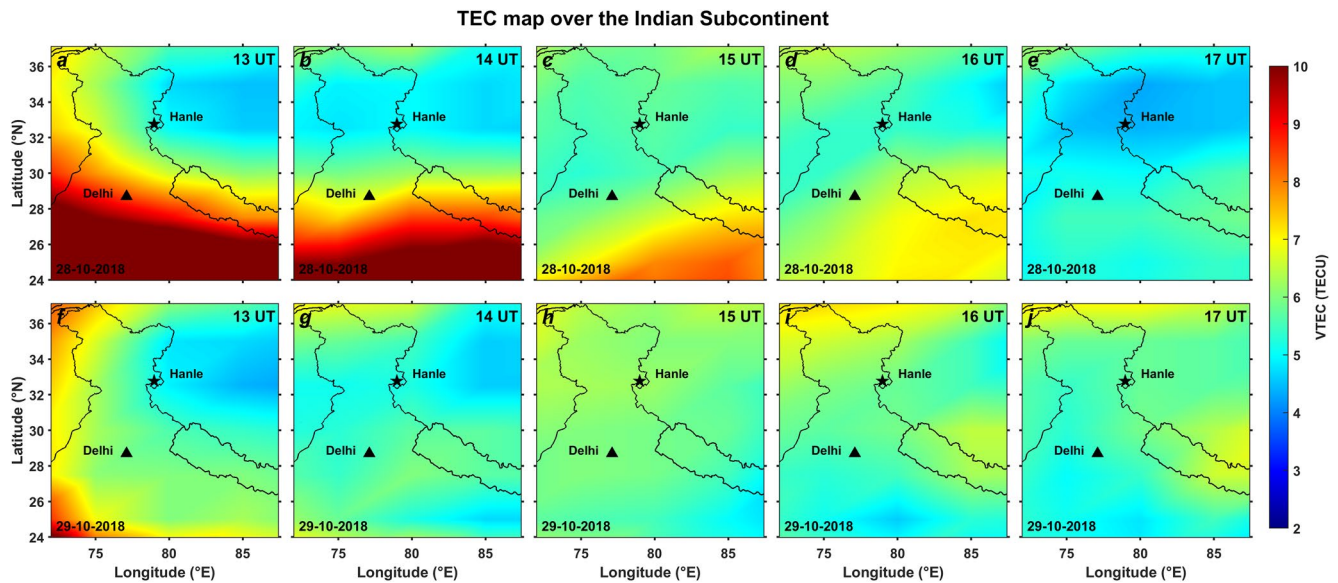
Figure 6. Hourly averaged global navigation satellite system (GNSS) total electron content (TEC) maps during October 28, 2018 (a–e) and October 29, 2018 (f–j) from 13:00 to 17:00 UT over the northern part of Indian subcontinent. The location of Hanle (star) and New Delhi (triangle) are indicated in the figures.

4.2. Role of Reduced TEC Over Southern Part of Onset Region

Recently, Sivakandan et al. (2019) argued that low electron density in the low latitude region may support the ingression of the mid-latitude MSTIDs and/or FAIs to the low latitudes by reducing the short-circuiting effect. Therefore, the role of F region electron density distribution in the onset of depletion is investigated in this case by using the global TEC maps. In Figure 6, top and bottom panels display the global TEC maps from 13:00 to 17:00 UT over the Indian sectors on October 28 and 29, 2018 respectively. Interestingly, the TEC on 29 October 2018 is lesser compared to October 28, 2018 on the southern side of FOV of the imager particularly during 13:00–16:00 UT. The importance of this argument can be gauged from the fact that the Es layers are also present on October 28, 2018 similar to October 29, 2018. Moreover, similar to October 29, 2018, h'F started going up from 14:20 UT on October 28, 2018 also as can be observed from the ionograms in the Figure 4. However, no clear spread F activity is seen on October 28, 2018. Therefore, despite the presence of conducive seeding (Es activities) and background (upward drift of the F layer base) conditions, spread-F did not occur on October 28, 2018. This suggests that the enhanced TEC and hence enhanced flux-tube integrated conductivity (Pedersen conductivity in the F region is directly proportional to the electron density) on the southern side of New Delhi on October 28, 2018 might have played a role in enhancing the short-circuiting effect of the polarization electric field that is needed for a depletion to grow.

Therefore, in order to summarize and synthesize the above observations, we made a simple schematic diagram of geomagnetic field line mapping of E and F region that is shown in the Figure 7. This figure showcases the possible physical mechanisms that are needed to explain the generation of the plasma depletion structure on October 29, 2018. In this schematic diagram, Es layer (~100 km) over New Delhi's latitude, base of the F layer (~220 km), airglow emission layer and F region electron density peak (~350 km) are highlighted in yellow, magenta, red, and light green respectively. The Es layer and onset of depletion at the base of the F layer as well as the latitude of New Delhi and Hanle also marked by the star symbols. Furthermore, the onset and the evolution of plasma bubble perpendicular to the magnetic field line is shown in a magenta plume. The black lines denote the magnetic field lines (aligned in the NS direction). These geomagnetic field line mapping have been carried out using IGRF model (Alken et al., 2021) outputs. This schematic also depicts that the onset of the plasma bubble occurred south of New Delhi's latitude by the coupled Es and F region instabilities. Earlier investigation by Cosgrove and Tsunoda (2003 and reference cited therein) showed that the larger effects due to Es layer polarization electric field should arise when the F layer conductance is smaller. This suggests that the field line integrated Pedersen conductivity in the north of onset location (Σ_{PN}) is relatively smaller in this case that facilitated the mapping of the seed
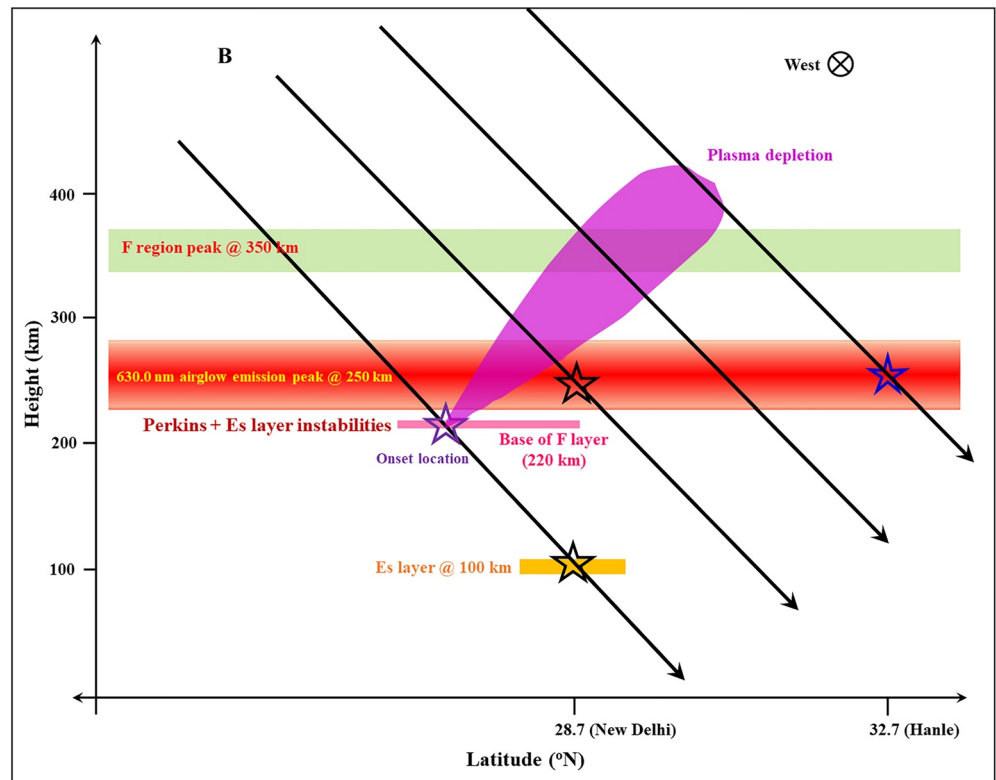
Figure 7. Schematic diagram of Es layer F region coupling over Hanle (Not to Scale). The Es layer and onset of depletion at the base of the F layer as well as the latitude of New Delhi and Hanle also marked by the star symbols.

perturbation in the electric field from the Es layer to the bottomside of the F region over the onset region. We go one step further and suggest that not only the reduced flux tube conductivity (E and F layer) in the northern side of onset location is important but also the reduced flux tube integrated F region conductivity (as suggested by the TEC map on this night) on the southern side of onset location (Σ_{PS}) is equally important to facilitate the growth of the plasma depletion structure captured by the imager in the present case. This can happen if the Es layer north of the onset location of the bubble, the bottomside of the plasma depletion structure at the onset location and the peak of the F region south of the onset location remain in the same flux tube. Therefore, the present investigation seems to suggest that the reduced conductivity south of the onset location is an equally important background condition as that of intense Es layer for the generation of plasma irregularities over the geomagnetic low-mid latitude transition region.

5. Conclusion

The onset of plasma depletion structures is captured over a geomagnetic low-mid latitude station on a geomagnetic quiet night for the first-time using an all-sky airglow imager. It is proposed that a combination of Perkins instability in the F region and possible Es layer instabilities through E-F region coupling have played important role in the development of the plasma depletion structures within around 25 min. It is also suggested that the reduced flux-tube integrated F region conductivity south of the onset region has played an important role in the development of the plasma depletion structure on this night. This investigation thus suggests that a complex interplay of several factors contribute to the development of the plasma depletion structure at the transition region geomagnetic of low-mid latitudes.

Data Availability Statement

The TEC map over the Indian subcontinent has been downloaded from Space Physics Data Facility, Goddard Space Flight Center (https://cdaweb.gsfc.nasa.gov/index.html). GNSS RINEX files for the GNSS-TEC processing are provided from many organizations listed by the webpage (http://stdb2.isee.nagoya-u.ac.jp/GPS/GPS-TEC/gnss_provider_list.html). The all-sky unwarpped images over Hanle, ROTI and New Delhi ionogram data are available at https://doi.org/10.5281/zenodo.4020314.

References

Alken, P., Thebault, E., Beggan, C., Amit, H., Aubert, J., Baerenzung, J., et al. (2021). International geomagnetic reference field: The thirteenth generation. *Earth Planets and Space*, *73*, 50. https://doi.org/10.1186/s40623-020-01288-x

Behnke, R. (1979). F layer height bands in the Nocturnil ionosphere over Arecibo. *Journal of Geophysical Research*, *84*(8), 974–978. https://doi.org/10.1029/JA084iA03p00974

Bowman, G. G. (1990). A review of some recent work on mid-latitude spread-F occurrence as detected by ionosondes. *Journal of Geomagnetism and Geoelectricity*, *42*(2), 109–138. https://doi.org/10.5636/jgg.42.109

Bowman, G. G., & Monro, P. E. (1988). Mid-latitude range spread and travelling ionospheric disturbances. *Journal of Atmospheric and Terrestrial Physics*, *50*(3), 215–223. https://doi.org/10.1016/0021-9169(88)90070-0

Chiu, Y. T., & Straus, J. M. (1979). Rayleigh-Taylor and wind driven instabilities of the nighttime equatorial ionosphere. *Journal of Geophysical Research*, *84*(8), 3283–3290. https://doi.org/10.1029/JA084iA07p03283

Cosgrove, R. (2013). Mechanisms for E-F coupling and their manifestation. *Journal of Atmospheric and Solar-Terrestrial Physics*, *103*, 56–65. https://doi.org/10.1016/j.jastp.2013.03.011

Cosgrove, R. B. (2007). Generation of mesoscale F layer structure and electric fields by the combined Perkins and Es layer instabilities, in simulations. *Annales Geophysicae*, *25*(7), 1579–1601. https://doi.org/10.5194/angeo-25-1579-2007

Cosgrove, R. B., & Tsunoda, R. T. (2001). Polarization electric fields sustained by closed-current dynamo structures in midlatitude sporadic E. *Geophysical Research Letters*, *28*, 1455–1458. https://doi.org/10.1029/2000GL012178

Cosgrove, R. B., & Tsunoda, R. T. (2002). Wind-shear-driven, closed-current dynamos in midlatitude sporadic E. *Geophysical Research Letters*, *29*(2). https://doi.org/10.1029/2001GL013697

Cosgrove, R. B., & Tsunoda, R. T. (2003). Simulation of the nonlinear evolution of the sporadic- E layer instability in the nighttime midlatitude ionosphere. *Journal of Geophysical Research*, *108*(A7), 1283. https://doi.org/10.1029/2002JA009728

Cosgrove, R. B., & Tsunoda, R. T. (2004). Instability of the E-F coupled nighttime midlatitude ionosphere. *Journal of Geophysical Research*, *109*(A4), 1–7. https://doi.org/10.1029/2003JA010243

Cosgrove, R. B., Tsunoda, R. T., Fukao, S., & Yamamoto, M. (2004). Coupling of the Perkins instability and the sporadic E layer instability derived from physical arguments. *Journal of Geophysical Research*, *109*(A6), 1–11. https://doi.org/10.1029/2003JA010295

Ding, F., Wan, W., Xu, G., Yu, T., Yang, G., & Wang, J. S. (2011). Climatology of medium-scale traveling ionospheric disturbances observed by a GPS network in central China. *Journal of Geophysical Research*, *116*(9), 1–11. https://doi.org/10.1029/2011JA016545

Earle, G. D., Bhaneja, P., Roddy, P. A., Swenson, C. M., Barjatya, A., Bishop, R. L., et al. (2010). A comprehensive rocket and radar study of midlatitude spread F. *Journal of Geophysical Research*, *115*(12), 1–21. https://doi.org/10.1029/2010JA015503

Fukao, S., Kelley, M. C., Shirakawa, T., Takami, T., Yamamoto, M., Tsuda, T., & Kato, S. (1991). Turbulent upwelling of the mid-latitude ionosphere: 1. Observational results by the MU radar. *Journal of Geophysical Research*, *96*(A3), 3725. https://doi.org/10.1029/90JA02253

Haldoupis, C., Kelley, M. C., Hussey, G. C., & Shalimov, S. (2003). Role of unstable sporadic-E layers in the generation of midlatitude spread F. *Journal of Geophysical Research*, *108*(A12), 1–8. https://doi.org/10.1029/2003JA009956

Huang, C.-S., & Kelley, M. C. (1996). Nonlinear evolution of equatorial spread F 1. On the role of plasma instabilities and spatial resonance associated with gravity wave seeding. *Journal of Geophysical Research*, *3*(3), 283–292. https://doi.org/10.1029/95JA02211

Hysell, D., Larsen, M., Fritts, D., Laughman, B., & Sulzer, M. (2018). Major upwelling and overturning in the mid-latitude F region ionosphere. *Nature Communications*, *9*(1), 3326. https://doi.org/10.1038/s41467-018-05809-x

Hysell, D. L., Larsen, M., & Sulzer, M. (2016). Observational evidence for new instabilities in the midlatitude E and F region. *Annales Geophysicae*, *34*(11), 927–941. https://doi.org/10.5194/angeo-34-927-2016

Ji, S., Chen, W., Weng, D., & Wang, Z. (2015). Characteristics of equatorial plasma bubble zonal drift velocity and tilt based on Hong Kong GPS CORS network: From 2001 to 2012. *Journal of Geophysical Research: Space Physics*, *120*(8), 7021–7029. https://doi.org/10.1002/2015JA021493-T

Kelley, M. (2009). *The Earth's ionosphere: Plasma physics and electrodynamics* (Vol. 96, pp.145). Boston, MA: Elsevier, Academic Press.

Larsen, M. F., Hysell, D. L., Zhou, Q. H., Smith, S. M., Friedman, J., & Bishop, R. L. (2007). Imaging coherent scatter radar, incoherent scatter radar, and optical observations of quasiperiodic structures associated with sporadic E layers. *Journal of Geophysical Research*, *112*(6), 1–12. https://doi.org/10.1029/2006JA012051

Makela, J. J., & Kelley, M. C. (2003). Using the 630.0-nm nightglow emission as a surrogate for the ionospheric Pedersen conductivity. *Journal of Geophysical Research*, *108*(A6), 1253. https://doi.org/10.1029/2003JA009894

Makela, J. J., Kelley, M. C., González, S. A., Aponte, N., & McCoy, R. P. (2001). Ionospheric topography maps using multiple-wavelength all-sky images. *Journal of Geophysical Research*, *106*(A12), 29161–29174. https://doi.org/10.1029/2000JA000449

Mathews, J. D., González, S., Sulzer, M. P., Zhou, Q. H., Urbina, J., Kudeki, E., & Franke, S. (2001). Kilometer-scale layered structures inside spread-F. *Geophysical Research Letters*, *28*(22), 4167–4170. https://doi.org/10.1029/2001GL013077

McClure, J. P., Hanson, W. B., & Hoffman, J. H. (1977). Plasma bubbles and irregularities in the equatorial ionosphere. *Journal of Geophysical Research*, *82*(19), 2650–2656. https://doi.org/10.1029/JA082i019p02650

Miller, C. A., Swartz, W. E., Kelley, M. C., Mendillo, M., Nottingham, D., Scali, J., & Reinisch, B. (1997). Electrodynamics of midlatitude spread F 1. Observations of unstable, gravity wave-induced ionospheric electric fields at tropical latitudes. *Journal of Geophysical Research*, *102*(A6), 11521–11532. https://doi.org/10.1029/96JA03839

Mondal, S., Srivastava, A., Yadav, V., Sarkhel, S., Sunil Krishna, M. V., Rao, Y. K., & Singh, V. (2019). Allsky airglow imaging observations from Hanle, Leh Ladakh, India: Image analyses and first results. *Advances in Space Research*, *102*, 11521–11532. https://doi.org/10.1016/j.asr.2019.05.047

Narayanan, V. L., Shiokawa, K., Otsuka, Y., & Saito, S. (2014). Airglow observations of nighttime medium-scale traveling ionospheric disturbances from Yonaguni: Statistical characteristics and low-latitude limit. *Journal of Geophysical Research: Space Physics*, *119*(11), 9268–9282. https://doi.org/10.1002/2014JA020368

Otsuka, Y. (2018). Review of the generation mechanisms of post-midnight irregularities in the equatorial and low-latitude ionosphere. *Progress in Earth and Planetary Science*, *5*(1), 57. https://doi.org/10.1186/s40645-018-0212-7

Otsuka, Y., Shiokawa, K., Ogawa, T., Yokoyama, T., & Yamamoto, M. (2009). Spatial relationship of nighttime medium-scale traveling ionospheric disturbances and F region field-aligned irregularities observed with two spaced all-sky airglow imagers and the middle and upper atmosphere radar. *Journal of Geophysical Research*, *114*(5), 1–11. https://doi.org/10.1029/2008JA013902

Otsuka, Y., Tani, T., Tsugawa, T., Ogawa, T., & Saito, A. (2008). Statistical study of relationship between medium-scale traveling ionospheric disturbance and sporadic E layer activities in summer night over Japan. *Journal of Atmospheric and Solar-Terrestrial Physics*, *70*(17), 2196–2202.

Patra, A. K., Phanikumar, D. V., & Pant, T. K. (2009). Gadanki radar observations of F region field-aligned irregularities during June solstice of solar minimum: First results and preliminary analysis. *Journal of Geophysical Research*, *114*(12), 1–10. https://doi.org/10.1029/2009JA014437

Paulino, I., de Medeiros, A. F., Buriti, R. A., Takahashi, H., Sobral, J. H. A., & Gobbi, D. (2011). Plasma bubble zonal drift characteristics observed by airglow images over Brazilian tropical region. *Revista Brasileira de Geofísica*, *29*(2), 239–246. https://doi.org/10.1590/S0102-261X2011000200003

Perkins, F. (1973). Spread F and ionospheric currents. *Journal of Geophysical Research*, *78*(1), 218–226. https://doi.org/10.1029/JA078i001p00218

Rathi, R., Yadav, V., Mondal, S., Sarkhel, S., Sunil Krishna, M. V., & Upadhayaya, A. K. (2021). Evidence for simultaneous occurrence of periodic and single dark band MSTIDs over geomagnetic low-mid latitude transition region. *Journal of Atmospheric and Solar-Terrestrial Physics*, *215*, 105588. https://doi.org/10.1016/j.jastp.2021.105588

Saito, A., Iyemori, T., Sugiura, M., Maynard, N. C., Aggson, T. L., Brace, L. H., et al. (1995). Conjugate occurrence of the electric field fluctuations in the nighttime midlatitude ionosphere. *Journal of Geophysical Research*, *100*(A11), 21439–21451. https://doi.org/10.1029/95JA01505

Saito, S., Yamamoto, M., & Hashiguchi, H. (2008). Imaging observations of nighttime mid-latitude F-region field-aligned irregularities by an MU radar ultra-multi-channel system. *Annales Geophysicae*, *26*(8), 2345–2352. https://doi.org/10.5194/angeo-26-2345-2008

Sekar, R., & Chakrabarty, D. (2011). A review of the recent advances in the investigation of equatorial spread F and space weather effects over Indian sector using optical and other techniques, In *IAGA special sopron book series, "Aeronomy of the Earth's Atmosphere and Ionosphere"* (Vol. 2, pp. 251–268). https://doi.org/10.1007/978-94-007-0326-1_18

Sekar, R., Chakrabarty, D., Narayanan, R., & Patra, A. K. (2008). Thermospheric airglow intensity variations corresponding to various ESF structures revealed by VHF radar maps. *Annales Geophysicae*, *26*, 3863–3873.

Sekar, R., Chakrabarty, D., Narayanan, R., Sripathy, S., Patra, A. K., & Subbarao, K. S. V. (2004). Characterization of VHF radar observations associated with equatorial Spread F by narrow-band optical measurements. *Annales Geophysicae*, *22*, 3129–3136. Retrieved from http://www.ann-geophys.net/22/3129/2004/

Sekar, R., Kherani, E. A., Rao, P. B., & Patra, A. K. (2001). Interaction of two long-wavelength modes in the nonlinear numerical simulation model of equatorial Spread F. *Journal of Geophysical Research*, *106*, 24765–24775. https://doi.org/10.1029/2000JA000361

Shalimov, S., & Yamamoto, M. (2010). Influence of midlatitude sporadic E layer patches upon the F region plasma density. *Journal of Geophysical Research*, *115*(A5), A05309. https://doi.org/10.1029/2009JA014964

Shiokawa, K., Ihara, C., Otsuka, Y., & Ogawa, T. (2003). Statistical study of nighttime medium-scale traveling ionospheric disturbances using midlatitude airglow images. *Journal of Geophysical Research*, *108*(A1), 1–7. https://doi.org/10.1029/2002JA009491

Shiokawa, K., Otsuka, Y., Ihara, C., Ogawa, T., & Rich, F. J. (2003). Ground and satellite observations of nighttime medium-scale traveling ionospheric disturbance at midlatitude. *Journal of Geophysical Research*, *108*, 1145. https://doi.org/10.1029/2002JA009639

Sivakandan, M., Chakrabarty, D., Ramkumar, T. K., Guharay, A., Taori, A., & Parihar, N. (2019). Evidence for deep ingression of the midlatitude MSTID into as low as ~3.5° magnetic latitude. *Journal of Geophysical Research: Space Physics*, *124*(1), 749–764. https://doi.org/10.1029/2018JA026103

Sivakandan, M., Mondal, S., Sarkhel, S., Chakrabarty, D., Sunil Krishna, M. V., Chaitanya, P. P., et al. (2020). Mid-latitude spread-F structures over the geomagnetic low-mid latitude transition region: An observational evidence. *Journal of Geophysical Research: Space Physics*, *125*(5), 1–13. https://doi.org/10.1029/2019JA027531

Sun, L., Xu, J., Wang, W., Yuan, W., Li, Q., & Jiang, C. (2016). A statistical analysis of equatorial plasma bubble structures based on an all-sky airglow imager network in China. *Journal of Geophysical Research: Space Physics*, *121*, 11495–11517. https://doi.org/10.1002/2016JA022950

Sun, L., Xu, J., Wang, W., Yue, X., Yuan, W., Ning, B., et al. (2015). Mesoscale field-aligned irregularity structures (FAIs) of airglow associated with medium-scale traveling ionospheric disturbances (MSTIDs). *Journal of Geophysical Research - A: Space Physics*, *120*(11), 9839–9858. https://doi.org/10.1002/2014JA020944

Swartz, W. E., Kelley, M. C., Makela, J. J., Collins, S. C., Kudeki, E., Franke, S., et al. (2000). Coherent and incoherent scatter radar observations during intense mid-latitude spread F. *Geophysical Research Letters*, *27*(18), 2829–2832. https://doi.org/10.1029/2000GL000021

Taori, A., & Sindhya, A. (2014). Measurements of equatorial plasma depletion velocity using 630 nm airglow imaging over a low-latitude Indian station. *Journal of Geophysical Research: Space Physics*, *119*(1), 396–401. https://doi.org/10.1002/2013JA019465

Tsugawa, T., Otsuka, Y., Coster, A. J., & Saito, A. (2007). Medium-scale traveling ionospheric disturbances detected with dense and wide TEC maps over North America. *Geophysical Research Letters*, *34*(22), 1–5. https://doi.org/10.1029/2007GL031663

Tsunoda, R. T., & Cosgrove, R. B. (2001). Coupled electrodynamics in the nighttime midlatitude ionosphere. *Geophysical Research Letters*, *28*(22), 4171–4174. https://doi.org/10.1029/2001GL013245

Tsunoda, R. T., Livingston, R. C., McClure, J. P., & Hanson, W. B. (1982). Equatorial plasma bubbles: Vertically elongated wedges from the bottomside f layer. *Journal of Geophysical Research*, *87*, 9171–9180. https://doi.org/10.1029/JA087iA11p09171

Upadhayaya, A. K., & Mahajan, K. K. (2013). Ionospheric F 2 region: Variability and sudden stratospheric warmings. *Journal of Geophysical Research: Space Physics*, *118*(10), 6736–6750. https://doi.org/10.1002/jgra.50570

Woodman, R. F., & La Hoz, C. (1976). Radar observations of F region equatorial irregularities. *Journal of Geophysical Research*, *81*(31), 5447–5466. https://doi.org/10.1029/JA081i031p05447

Yadav, V., Rathi, R., Gaur, G., Sarkhel, S., Chakrabarty, D., Sunil Krishna, M. V., et al. (2021). Interaction between mid-latitude field aligned plasma structure and medium scale traveling ionospheric disturbances during nighttime over geomagnetic low-mid latitude transition region. *Journal of Atmospheric and Solar-Terrestrial Physics*, *217*, 105589. https://doi.org/10.1016/j.jastp.2021.105589

Yadav, V., Rathi, R., Sarkhel, S., Chakrabarty, D., Sunil Krishna, M. V., & Upadhayaya, A. K. (2021). A unique case of complex interaction between MSTIDs and mid-latitude field-aligned plasma depletions over geomagnetic low-mid latitude transition region. *Journal of Geophysical Research: Space Physics*, *126*(1), e2020JA028620. https://doi.org/10.1029/2020JA028620

Yao, D., & Makela, J. J. (2007). Analysis of equatorial plasma bubble zonal drift velocities in the Pacific sector by imaging techniques. *Annales Geophysicae*, *25*(3), 701–709. https://doi.org/10.5194/angeo-25-701-2007

Yokoyama, T., Hysell, D. L., Otsuka, Y., & Yamamoto, M. (2009). Three-dimensional simulation of the coupled Perkins and es-layer instabilities in the nighttime midlatitude ionosphere. *Journal of Geophysical Research: Space Physics*, *114*(3), 1–16. https://doi.org/10.1029/2008JA013789